

# Model-based Estimator Design for the Curing Process of a Concrete Structure<sup>★</sup>

Denis Ratke<sup>\*</sup> Thomas Meurer<sup>\*</sup> Yannik Schwarz<sup>\*\*</sup>  
David Sanio<sup>\*\*</sup> Peter Mark<sup>\*\*</sup>

<sup>\*</sup> *Digital Process Engineering Group, Institute of Mechanical Process Engineering and Mechanics, Karlsruhe Institute of Technology, 76187 Karlsruhe, Germany (e-mail: {denis.ratke, thomas.meurer}@kit.edu).*

<sup>\*\*</sup> *Institute of Concrete Structures, Faculty of Civil and Environmental Engineering, Ruhr University Bochum, 44801 Bochum, Germany (e-mail: {yannik.schwarz, david.sanio, peter.mark}@ruhr-uni-bochum.de).*

**Abstract:** Concrete is one of the most important building materials and is used as a collective term for different dispersions of cement and aggregates. High performance concrete (HPC) is a rather new type of concrete mixture. A topic of current research is the behavior of fresh concrete during heat treatment. It is known that the heat treatment of fresh concrete accelerates the reaction of the cement and thus the chemically complex process of hydration. The mathematical representation of the curing concrete is a further step towards the systematic investigation. The objective of this work is the development of a state estimator to determine the temperature behavior of the fresh HPC mixture under heat treatment. Using a continuum representation describing the spatial-temporal evolution of temperature, moisture, and maturity of fresh HPC during heat treatment a finite-dimensional approximation is derived using a high order finite difference scheme. Experimental data is included for model parameterization by optimization. Based on this, three different nonlinear extensions of the Kalman filter (KF) techniques are realized and compared combining simulated and experimental data.

Copyright © 2023 The Authors. This is an open access article under the CC BY-NC-ND license (<https://creativecommons.org/licenses/by-nc-nd/4.0/>)

**Keywords:** Partial differential equations, Curing concrete, Civil engineering, Kalman filter, Nonlinear observer design, Parameter identification, Distributed parameter systems.

## 1. INTRODUCTION

High performance concrete (HPC) and ultra-high performance concrete (UHPC) are unique in terms of its special properties such as high strength and durability, see, e.g., Fehling et al. (2005). Due to its specific characteristics, the application of HPC and UHPC targets areas with extended requirements. Examples include its use in filigree bridge construction (Olipitz, 2015), anchoring system for prestressed bridge-slabs (Sanio et al., 2021) or for parabolic trough collectors (Forman et al., 2020)

Another potential of HPC can be exploited if it is subjected to heat treatment during the curing process. This results in faster achieved early strength and reduced shrinkage (Stindt et al., 2021). In addition to accelerated hardening by means of uniform heating of the total cross-section the imprinting of a temperature gradient across the cross-section is currently under investigation and initial experimental as well as theoretical investigations for adjusting the state of stress in bridges have been carried out by Löschmann and Mark (2022). Ideally, the accurate induction and control of temperature gradients requires knowledge of the temperature distribution of the entire cross-section. Here, the usage of fiber-optic measurement

sensors offers one possibility for temporal temperature measurement at a high spatial resolution (Clauß et al., 2022). Although this sensor allows accurate temperature measurement even inside a curing concrete structure high cost and the sensitivity limit its practical application.

Alternatively, a temperature estimate of the curing concrete body can be realized by a suitable mathematical model embedded in a software sensor. Examples of models of the concrete solidification process are provided in, e.g., Benedix (2011); Fowkes et al. (2004). Such models approximate the heating process of HPC based on thermal properties, chemical heat release, and suitable boundary conditions describing the interaction with the environment. Temperature and property estimation based purely on the open-loop simulation of numerical models is subject to error and deviation from the true value due to unknown initial conditions, parameter uncertainties, and modeling errors. As a consequence, a complementary online measurement – typically at easily accessible locations such as the surface edge points – coupled with a suitable state estimation technique can improve accuracy and enables us to reconstruct the spatial-temporal evolution of the state variables in real-time. Here, in particular the Kalman filter and its extensions to nonlinear systems seem appropriate providing a trade-off between implementation effort, robustness, estimation accuracy, and computation time (Gelb et al., 1974).

<sup>★</sup> The financial support by the Deutsche Forschungsgemeinschaft (DFG) in the project 458161128 (Mark/Meurer) is gratefully acknowledged.

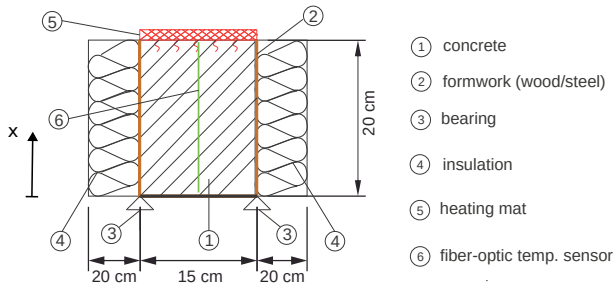


Fig. 1. Schematics of the experimental setup.

This work aims to provide a model-based estimation framework for the concrete curing and solidification process under external heating. For this a mathematical model in terms of coupled partial differential equations is introduced and approximated using the finite difference method. Relevant system parameters are identified using experimentally determined temperature data. Based on the parameterized discrete system, three Kalman filter approaches for the state estimation of nonlinear systems are designed, implemented, and evaluated, again based on experimental data.

The paper is organized as follows. Section 2 introduces the experimental setup. The mathematical model of curing HPC is presented in Section 3 together with a short summary of the used discretization scheme and the considered parameter identification. The theoretical details of the estimator designs are summarized in Section 4 and Section 5 provides an evaluation of the determined estimation scheme or software sensor, respectively. Final remarks conclude the paper.

## 2. EXPERIMENTAL SETUP

The hardening process of HPC with heating and its transient thermal properties are investigated. Thereby the concrete undergoes a change of state from liquid to solid. The concrete specimen consists of an HPC based on the binder Nanodur<sup>®</sup> Compound 5941 (Sagmeister, 2017). The cross-section of the experimental setup is shown in Fig. 1. The liquid HPC is filled into the formwork. The side walls are thermally insulated so that the heat dissipation can be considered negligible and the heat flow is almost one-dimensional. The base is formed by a steel plate so that the induced heat can dissipate almost undisturbed at the bottom. The top surface is closed with a silicone heating mat (max. 70 W output and on/off control) used as a heat source to accelerate process. The temperature in the concrete must not exceed 373.15 K to protect the concrete from damage (boiling of the unbound water). The concrete is tempered for 22.2 h at max 353.15 K. The concrete temperature inside the hardening material is measured by a fiber optic system, which is mounted in longitudinal direction inside capillaries almost over the entire length  $L \approx 0.194$  m of the body. The results, reduced by the initial temperature of 25 K, are given in Fig. 2 as the development of the temperature  $T$  in the concrete ( $x$  = longitudinal coordinate in the specimen, measurement point distance of  $\Delta x = 0.65$  mm) and over time (sampling rate 1 Hz). The temperature increases due to the external tempering. In addition, during the hardening process, so-called hydration heat is released,

which is superimposed on the externally induced heat. The maximum temperature is reached in the concrete after about 10 hours. Afterwards, the hydration heat dissipates, and a steady-state temperature distribution is established. The setup was developed, and experiments were carried out at the Institute of Concrete Structures at the Ruhr University Bochum, Germany. It should be mentioned that the considered setup is used as a benchmark in view of the transfer of the approach to a real-world structure.

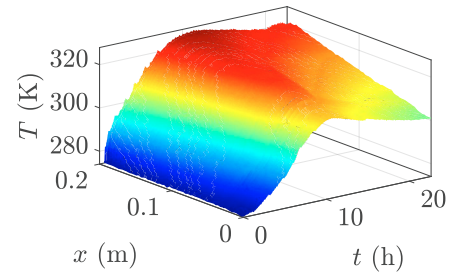


Fig. 2. Spatial-temporal temperature profile measured for 22.2 h over the length of the concrete body.

## 3. MATHEMATICAL MODEL

Concrete curing is a rather complicated thermo-chemical process involving different dynamical effects. In the following the model introduced by Myers and Charpin (2008) is considered, which consists of three coupled partial differential equations (PDEs)

$$\rho c_p \partial_t T = \partial_x (\lambda(m) \partial_x T) + \partial_t Q, \quad (1a)$$

$$\partial_t \theta = \partial_x (D(\theta) \partial_x \theta) - \eta \partial_t m, \quad (1b)$$

$$\partial_t m = \mu (1 - m) \theta e^{-E/RT} \quad (1c)$$

defined on the domain  $\Omega = \{(x, t) : x \in [0, L], t \in [0, \bar{t}]\}$ . Note that due to symmetry only the evolution along the  $x$ -direction is considered. Herein  $T(x, t)$ ,  $\theta(x, t)$ , and  $m(x, t)$  represent temperature, (relative) moisture, and (degree of) maturity, respectively. The maturity  $m(x, t)$  reflects the degree of hydration and is the solution of (1c). The thermal material properties are defined by means of heat capacity  $c_p$ , conductivity  $\lambda(m)$ , and material density  $\rho$ . The nonlinear behavior of moisture diffusion in the concrete is determined by the relation

$$D(\theta) = D_m [0.05 + 0.95(1 + \tanh(20(\theta - 0.8)))] \quad (2)$$

with coefficient  $D_m$  as the amplitude, see Myers and Charpin (2008). The hydration heat release is given by the source term

$$\partial_t Q = Q_m \partial_t m, \quad Q_m = A m e^{-am^2}, \quad (3)$$

where  $a = 1/2m_x^2$  and  $A = Q_x/m_x$  with  $m_x$  the value  $m$  for  $Q_m$  reaching its maximum  $Q_x$ . The hydration reaction ratio  $\eta$  represents the sink term of the moisture equation. The parameters  $E$ ,  $R$ , and  $\mu$  represent activation energy, gas-constant and reaction-rate. The PDEs (1) are equipped with initial conditions

$$T(x, 0) = T_0(x), \quad \theta(x, 0) = \theta_0(x), \quad m(x, 0) = m_0(x) \quad (4)$$

and boundary conditions

$$\begin{aligned}
 -\lambda(m)\partial_x T|_{x=0} &= \sigma_1(T(x,t) - T_{1,\infty}), & (5a) \\
 \lambda(m)\partial_x T|_{x=L} &= \sigma_2(T(x,t) - T_{2,\infty}), & (5b) \\
 -D(\theta)\partial_x \theta|_{x=0} &= \bar{e}(\theta_a - \theta(L,t)), & (5c) \\
 D(\theta)\partial_x \theta|_{x=L} &= 0, & (5d)
 \end{aligned}$$

which result from the experimental setup and the assumptions that  $m(x,t) \in [0, 1]$ ,  $\theta(x,t) \in [0, 1]$ . Here,  $\sigma_1$  and  $\sigma_2$  denote the heat transfer coefficients,  $T_{1,\infty}$ ,  $T_{2,\infty}$  refer to the ambient temperature at  $x \in \{0, L\}$ , the  $\theta_a$  is the ambient moisture and  $\bar{e}$  is the rate of evaporation.

### 3.1 Discretization Scheme

The system composed of (1)-(5) can be approximated using a finite difference method on a uniform spaced grid with  $n_x, n_t \in \mathbb{N}$  the number of grid points in space and time, respectively. The spatial and temporal step lengths are defined by  $\Delta x = L/n_x$  and  $\Delta t = \bar{t}/n_t$ . Temperature, moisture, and maturity at the grid points  $x_i = i\Delta x$ ,  $i = 0, 1, \dots, n_x$  and  $t_k = k\Delta t$ ,  $k = 0, 1, \dots, n_t$  are denoted  $T_{i,k}$ ,  $\theta_{i,k}$ , and  $m_{i,k}$ , respectively. For numerical stability purposes a combination of an implicit and explicit discretization for (1) is used involving a Crank-Nicholson scheme for the time derivatives and a central difference method for the spatial derivatives, see, e.g., Schwarz and Köckler (2009). The parameters  $\lambda(m)$ ,  $D(\theta)$  are discretized with an explicit method. This results in

$$E_k \mathbf{T}_{k+1} = A_k \mathbf{T}_k + \mathbf{u}_{T,k}, \tag{6a}$$

$$U_k \boldsymbol{\theta}_{k+1} = Y_k \boldsymbol{\theta}_k + \mathbf{u}_{\theta,k}, \tag{6b}$$

$$\mathbf{m}_{k+1} = \mathbf{m}_k + \Delta t \mu (1 - \mathbf{m}_k) \boldsymbol{\theta}_k e^{-\frac{E}{RT_k}}, \tag{6c}$$

where  $E_k \in \mathbb{R}^{n_x \times n_x}$ ,  $A_k \in \mathbb{R}^{n_x \times n_x}$ ,  $U_k \in \mathbb{R}^{n_x \times n_x}$ ,  $Y_k \in \mathbb{R}^{n_x \times n_x}$  are tri-diagonal matrices resulting from spatial and implicit-explicit time discretization, which are recalculated at each time step  $k$  with the initial conditions  $\mathbf{T}_0$ ,  $\boldsymbol{\theta}_0$  and  $\mathbf{m}_0$ . The input vectors  $\mathbf{u}_{T,k} \in \mathbb{R}^{n_x}$ ,  $\mathbf{u}_{\theta,k} \in \mathbb{R}^{n_x}$  are obtained from the explicit discretization of the source and sink terms and the incorporation of the boundary conditions. Let  $\mathbf{T}_k = [T_{0,k}, \dots, T_{n_x,k}]^T$ ,  $\boldsymbol{\theta}_k = [\theta_{0,k}, \dots, \theta_{n_x,k}]^T$  and  $\mathbf{m}_k = [m_{0,k}, \dots, m_{n_x,k}]^T$  be the respective state vectors. Then (6) admits a representation in the general form

$$\mathbf{z}_{k+1} = \mathbf{f}(\mathbf{z}_k, \mathbf{u}_k), \tag{7}$$

with state vector  $\mathbf{z}_k = [\mathbf{T}_k^T, \boldsymbol{\theta}_k^T, \mathbf{m}_k^T]^T \in \mathbb{R}^n$  and input vector  $\mathbf{u} = [\mathbf{u}_{T,k}^T, \mathbf{u}_{\theta,k}^T]^T \in \mathbb{R}^n$  for  $n = 3(n_x + 1)$ .

### 3.2 Parameter Identification

Parameter identification is performed to estimate the values of  $c_p$ ,  $\mu$ ,  $D_m$ ,  $\eta$ ,  $m_x$ ,  $Q_x$ ,  $\sigma_1$ ,  $\sigma_2$  and  $T_{1,\infty}$  as well as the functional relation of the conductivity  $\lambda(m)$ . As the heat mat doesn't have direct contact with concrete, adjusting  $T_{2,\infty}$  becomes both a parameter to search and heat input. All other parameters were taken from Myers and Charpin (2008). Table 3.2 summarizes both the used literature and the identified parameters. The identification was carried out using `fmincon` in MATLAB by minimizing the magnitude of the Euclidean distance between the measured and numerically calculated temperatures. Note that at the experiment it is currently not possible to measure any value of  $\theta$  and  $m$ . In addition, the determination of the thermal conductivity is necessary. For this different ansatz functions have been investigated to represent the

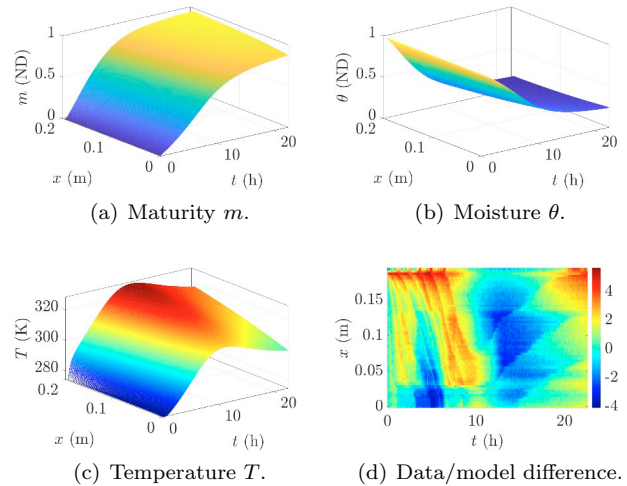


Fig. 3. Numerical solution of (7) for the parameters of Table 3.2 and the error between measured and numerically calculated temperature.

dependency of  $\lambda$  on the maturity  $m$  eventually leading to the formulation

$$\lambda(m) = \lambda_0(1 + \exp(-m)), \tag{8}$$

with  $\lambda_0$  adjusted to minimize the distance to the experimental results. The solution of (7) with parameters from

Table 1. System parameters.

Symbol	Value	Units	Symbol	Value	Units
$\rho$	2440	kg/m <sup>3</sup>	$c_p$	1320	J/(kg K)
$\lambda_0$	2.3	W/(K m)	$D_m$	10 <sup>9</sup>	m <sup>2</sup> /s
$\eta$	2	ND	$\mu$	50	1/s
$R$	8.314	J/K	$E$	35	kJ
$Q_x$	10 <sup>8</sup>	J/m <sup>3</sup>	$m_x$	0.1	ND
$\sigma_1$	16	W/(K m <sup>2</sup> )	$\sigma_2$	20.5	W/(K m <sup>2</sup> )
$\bar{e}$	0.02	m/s	$T_{2,\infty}$	334.5	K
$T_{1,\infty}$	276	K	-	-	-

Table 3.2 is shown in Fig. 3. The influence of hydration in the temperature pathway can be recognized as a bulge. Fig. 3(d) illustrated the results of the parameter estimation by building the difference between the experimentally recorded and by (6) calculated temperature with the parameters from Table 3.2.

## 4. NONLINEAR ESTIMATOR DESIGN

Monitoring the temperature inside a concrete block during the drying process is crucial to derive its internal properties such as stress. However, direct temperature measurement is often challenging and expensive. To address this issue, an observer is being developed to estimate the temperature using a mathematical model and measurements. The Kalman Filter is a potential method for designing such an observer, aiming to minimize the difference between the estimate and the true temperature value.

The classical KF is a discrete, linear estimation algorithm that is optimal when the process and measurement noise are modeled by Gaussian distribution. To deal with nonlinear problems various extensions of the KF have been proposed. In the following, three setups are addressed: extended Kalman filter (EKF), unscented Kalman filter

(UKF) and ensemble Kalman Filter (EnKF). The basic framework for the estimation algorithms involves a discrete-time nonlinear dynamic system

$$\mathbf{z}_{k+1} = \mathbf{f}(\mathbf{z}_k, \mathbf{u}_k) + \mathbf{w}_k \quad (9a)$$

$$\mathbf{y}_k = \mathbf{h}(\mathbf{z}_k) + \mathbf{v}_k, \quad (9b)$$

where  $\mathbf{z}_k$  represent the unobserved states of the system and  $\mathbf{y}_k \in \mathbb{R}^p$  the observed (measured) quantities. Moreover the additive process and observation noises  $\mathbf{w}_k \sim \mathcal{N}(0, Q)$  and  $\mathbf{v}_k \sim \mathcal{N}(0, R)$  are assumed to be zero mean Gaussian distributed with covariance matrices  $Q \in \mathbb{R}^{n \times n}$  and  $R \in \mathbb{R}^{p \times p}$ .

The Kalman filters are build upon the recursive forecast-analysis rule

$$\hat{\mathbf{z}}_{k+1} = \hat{\mathbf{z}}_{k+1}^- + K_k(\mathbf{y}_k - \mathbf{h}(\hat{\mathbf{z}}_{k+1}^-)) \quad (10)$$

where  $\hat{\mathbf{z}}_{k+1} \in \mathbb{R}^n$  is the current estimation as a result of the time prediction  $\hat{\mathbf{z}}_{k+1}^- = \mathbf{f}(\hat{\mathbf{z}}_k, \hat{\mathbf{u}}_k)$  by using the previous state estimate  $\hat{\mathbf{z}}_k$ , which is corrected by the innovation consisting of actual  $\mathbf{y}_k$  and predicted measurement  $\mathbf{h}(\hat{\mathbf{z}}_{k+1}^-)$  weighted with the Kalman gain matrix  $K_k$ . The Kalman gain is chosen to minimize the trace of the covariance of the estimation error, which yields

$$K_k = P_{\mathbf{z}\mathbf{y}}(P_{\mathbf{y}\mathbf{y}})^{-1} \quad (11)$$

with  $P_{\mathbf{z}\mathbf{y}} = \mathbb{E}[(\mathbf{z}_k - \hat{\mathbf{z}}_k^-)(\mathbf{y}_k - \hat{\mathbf{y}}_k^-)^T]$  the cross covariance matrix and  $P_{\mathbf{y}\mathbf{y}} = \mathbb{E}[(\mathbf{y}_k - \hat{\mathbf{y}}_k^-)(\mathbf{y}_k - \hat{\mathbf{y}}_k^-)^T]$  the covariance matrix.

#### 4.1 Extended Kalman Filter

The matrices  $P_{\mathbf{z}\mathbf{y}}$  and  $P_{\mathbf{y}\mathbf{y}}$  are determined based on the local linearization of the nonlinear equations around the current estimate using the Jacobians

$$F_k = \partial_{\mathbf{z}} \mathbf{f}(\hat{\mathbf{z}}_k, \mathbf{u}_k), \quad H_k = \partial_{\mathbf{z}} \mathbf{h}(\hat{\mathbf{z}}_k).$$

This results in the covariance matrices

$$P_{\mathbf{z}\mathbf{y}} = P_k^- H_k^T, \quad P_{\mathbf{y}\mathbf{y}} = H_k P_k^- H_k^T + R_k \quad (12)$$

with  $H_k \in \mathbb{R}^{p \times n}$  and  $P_k^- = F_k P_k F_k^T + Q_k$  as prior error covariance matrix, which consist the posterior error covariance  $P_k \in \mathbb{R}^{n \times n}$  and the Jacobian  $F_k \in \mathbb{R}^{n \times n}$ . For a detailed representation the reader is referred to, e.g., Welch and Bishop (2006).

#### 4.2 Unscented Kalman Filter

The UKF takes a different approach to handle the nonlinear processes. The idea is that instead of approximating a random nonlinear function, it is simpler to approximate the statistics of a random variable transformed by nonlinear function, see, e.g., Julier and Uhlmann (2004).

The approximation is obtained using the so-called unscented transformation. The approach is to deterministically select a set of  $2N + 1$  sigma points  $\mathcal{Z}_{j,k}$ ,  $j = 0, \dots, 2N$  with the mean  $\hat{\mathbf{z}}_{k+1}^-$  and covariance  $P_{\mathbf{z}\mathbf{z}}$ , e.g., by means of the method described in Wan and Van Der Merwe (2000). Then propagate the sigma points through the nonlinear function  $\mathcal{Y}_{j,k} = \mathbf{h}(\mathcal{Z}_{j,k})$  to determinate the statistics of the transformed points and to obtain the corresponding mean

$$\bar{\mathbf{y}}_k^- = \sum_{j=0}^{2N} W_j \mathcal{Y}_{j,k} \quad (13)$$

and the covariance matrices

$$P_{\mathbf{y}\mathbf{y}} = \sum_{j=0}^{2N} W_j (\mathcal{Y}_{j,k} - \bar{\mathbf{y}}_k^-)(\mathcal{Y}_{j,k} - \bar{\mathbf{y}}_k^-)^T, \quad (14a)$$

$$P_{\mathbf{z}\mathbf{y}} = \sum_{j=0}^{2N} W_j (\mathcal{Z}_{j,k+1} - \hat{\mathbf{z}}_{k+1}^-)(\mathcal{Y}_{j,k} - \bar{\mathbf{y}}_k^-)^T \quad (14b)$$

with an appropriate weight  $W_j$  (Julier and Uhlmann, 2004). Using (14) the Kalman gain  $K_k$  can be computed to update the estimate by means of the current measurement.

#### 4.3 Ensemble Kalman Filter

Using ensemble integration the EnKF is a sequential data assimilation method to calculate the mean and error covariances by integrating an ensemble of model states forward in time. The EnKF scheme used in this work is taken from the Gillijns et al. (2006).

Similar to the UKF, a set of points, the so-called ensembles, is used to determine the process statistics. In contrast to the Unscented transformation the method for the determination of the ensembles is not firmly defined so that typically some randomized sequence is considered, for more details on the determination of the ensembles, see, e.g., Evensen (2003). Starting with the ensembles

$$\mathbf{Z}_{k+1} = [\hat{\mathbf{z}}_{1,k+1}^-, \dots, \hat{\mathbf{z}}_{q,k+1}^-] \in \mathbb{R}^{n \times q} \quad (15)$$

of forecasted state estimates  $\hat{\mathbf{z}}_{l,k+1}^-$ , where  $l$  denotes the  $l$ -th ensemble, the ensemble mean is determined

$$\bar{\mathbf{z}}_{k+1}^- = \frac{1}{q} \sum_{l=0}^q \hat{\mathbf{z}}_{l,k+1}^-. \quad (16)$$

The latter is used to approximate the cross correlation and innovation covariance matrices

$$P_{\mathbf{z}\mathbf{y}} = \frac{1}{q-1} E_k (E_{\mathbf{y}_k})^T \quad (17a)$$

$$P_{\mathbf{y}\mathbf{y}} = \frac{1}{q-1} E_{\mathbf{y}_k} (E_{\mathbf{y}_k})^T \quad (17b)$$

by using the ensemble error  $E_{\mathbf{z}} \in \mathbb{R}^{n \times q}$  and the output error matrix  $E_{\mathbf{y}} \in \mathbb{R}^{p \times q}$  with respect to the ensemble mean, i.e.,

$$E_{\mathbf{z}} = [\hat{\mathbf{z}}_{1,k+1}^- - \bar{\mathbf{z}}_{k+1}^-, \dots, \hat{\mathbf{z}}_{q,k+1}^- - \bar{\mathbf{z}}_{k+1}^-] \quad (18a)$$

$$E_{\mathbf{y}} = [\hat{\mathbf{y}}_{1,k}^- - \bar{\mathbf{y}}_k^-, \dots, \hat{\mathbf{y}}_{q,k}^- - \bar{\mathbf{y}}_k^-]. \quad (18b)$$

Herein  $\hat{\mathbf{y}}_{l,k}^-$  refers to the propagation of the ensembles by the nonlinear function  $\mathbf{h}(\hat{\mathbf{z}}_{l,k+1}^-)$  and  $\bar{\mathbf{y}}_k^-$  is the corresponding mean computed similar to (16). Subsequently the state estimation can be performed with the recursive rule (10) by using the covariance matrices (17) to form the Kalman gain (11).

## 5. RESULTS

The performance of the nonlinear estimators is evaluated in two scenarios making use of recorded temperature data sets from experiments. For the discretized model (6) or (7), respectively,  $n_x = 61$  and  $n_t = 1001$  is chosen given  $L \approx 0.194$  m and end time  $\bar{t} = 22.2$  h. The data set I corresponds to the set used for parameter identification. Data set II is used here as validation data set. Although the two sets were recorded under similar conditions, certain

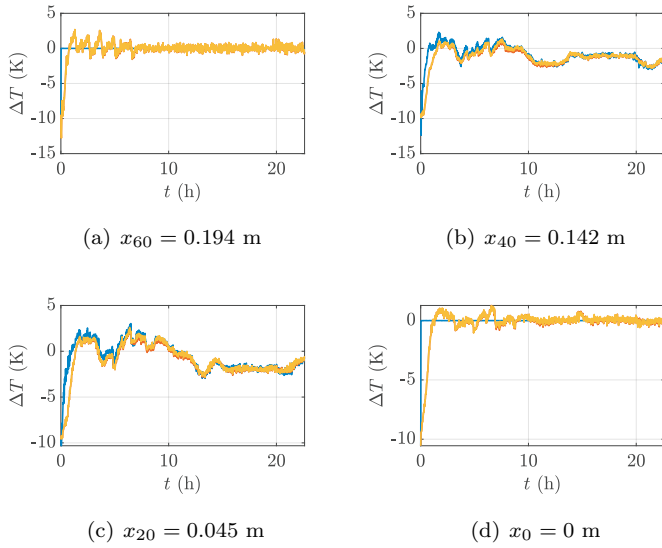


Fig. 4. Scenario A: Evolution of estimation error for — EnKF, — UKF, — EKF for data set I.

differences exist. In particular concrete mixes from different batches are considered and the ambient conditions vary slightly.

5.1 Scenario A

For the first scenario, it is assumed that two point sensors for recording the temperature are placed at the upper  $i = 0$  and lower  $i = n_x$  boundary points so that only the temperatures  $\hat{T}_0$  and  $\hat{T}_{n_x}$  are measured. To evaluate the estimators an incorrect initial estimate for temperature  $\mathbf{T}_0 = [285, \dots, 285]^T$  K, moisture  $\boldsymbol{\theta}_0 = [0.99, \dots, 0.99]^T$ , and maturity  $\mathbf{m}_0 = [0.005, \dots, 0.005]^T$  is provided. To ensure comparability of the EKF and UKF identical (constant) covariance matrices  $Q_k = Q = 4 \times 10^{-4} I_n$ ,  $R_k = R = \text{diag}(0.36, 0.216)$ , and  $P_0 = 10^{-3} I_n$  are used, where  $I_n$  is the identity matrix of size  $\mathbb{R}^{n \times n}$ . To achieve a numerically stable estimate with the EnKF,  $Q = \text{diag}(0.05 I_{n_x}, 0.45 I_{n_x}, 10^{-4} I_{n_x})$  and  $R = \text{diag}(0.05, 0.05)$  are assigned considering  $q = 200$  ensembles.

Estimation results are shown in Fig. 4 for data set I and in Fig. 5 for data set II. Here the evolution of temperature estimation error, i.e., the difference between the measured and the estimated temperature, is illustrated for the three Kalman filters at four different locations. Obviously the performance of all estimators is almost identically good. The EnKF shows a slightly faster convergence. As  $x_0$  and  $x_{60}$  refer to the measurement locations the estimation error, after some initial transients, is smallest. However, the temperature inside the body during the curing and solidification process is still accurately reconstructed. For the validation data set II, which is not used in the parameter identification, Fig. 5 confirms that all nonlinear estimators are capable to accurately reconstruct the temperature evolution at the boundaries and inside the body. In addition, both moisture and maturity can be estimated online. For these, currently no measurements are available. The resulting curves obtained from the EnKF for data set I is presented in Fig. 6. Both, moisture and maturity, show an opposite behavior and reflect the progress of the

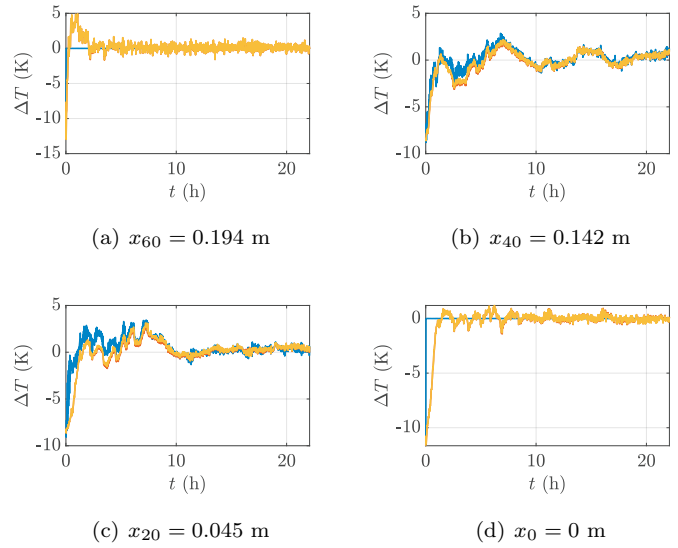


Fig. 5. Scenario A: Evolution of estimation error for — EnKF, — UKF, — EKF for data set II.

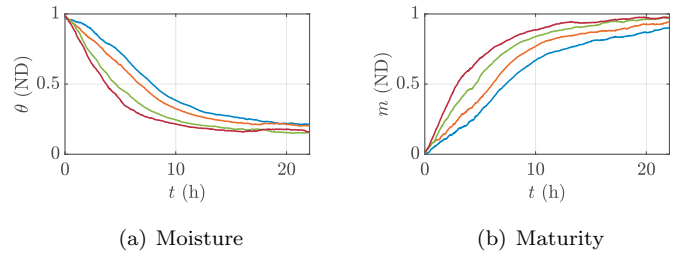


Fig. 6. Estimation of moisture and maturity obtained from the EnKF for —  $x_0 = 0$  m, —  $x_{20} = 0.045$  m, —  $x_{40} = 0.142$  m and —  $x_{60} = 0.194$  m for data set I.

hydration. The curves for the different positions show that the heating of the concrete leads to an acceleration of the hydration and hence also the solidification. The concrete near the heating mat hydrates faster.

5.2 Scenario B

Differing from Scenario A only a single pointwise temperature measurement at the upper boundary  $x = L$  or  $x_{n_x-1} = x_{60}$  is considered. The initial conditions for the estimators and covariance matrices  $Q$  and  $P_0$  are those of Scenario A. However,  $R = 0.216$  and  $R = 0.05$  for the EKF/UKF and the EnKF are considered. It becomes apparent from Fig. 7 for data set I and Fig. 8 for data set II showing the estimation errors at different locations that the nonlinear estimation schemes are still able to accurately approximate the measure temperature evolution. As expected, the reduced information implies a slightly larger error and in parts reduces influences the estimator convergence, in particular for locations with increasing distance to the sensor position. Nevertheless, the estimation error remains in an acceptable range for all algorithms.

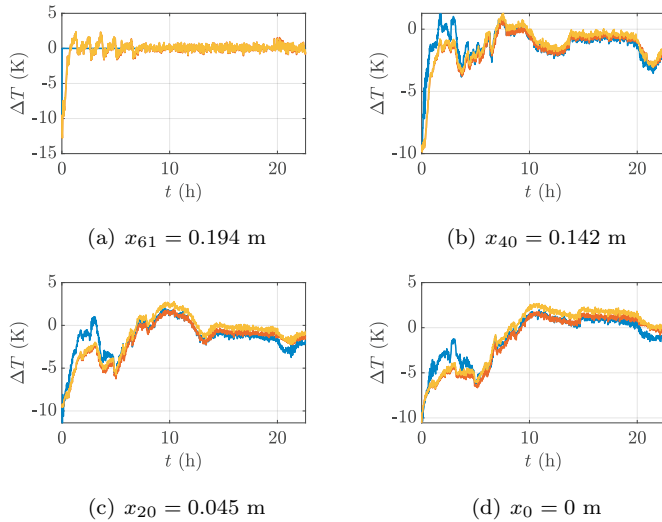


Fig. 7. Scenario B: Evolution of estimation error for — EnKF, — UKF, — EKF for data set I.

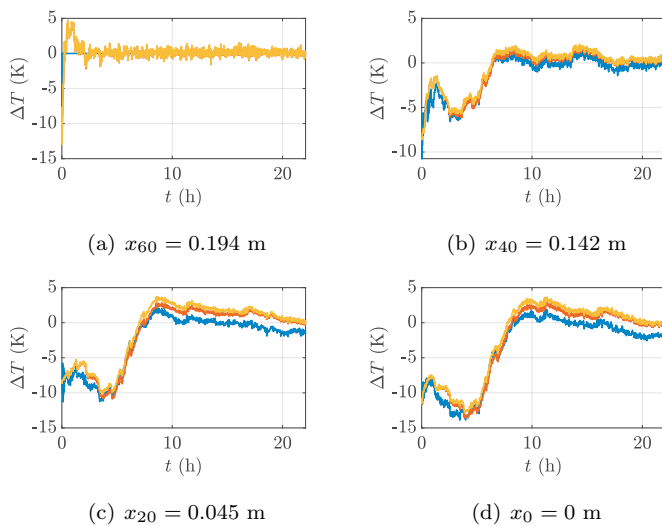


Fig. 8. Scenario B: Evolution of estimation error for — EnKF, — UKF, — EKF, for data set II.

## 6. CONCLUSIONS

The model-based state estimation problem for concrete curing and solidification under external heating has been addressed and validated in numerical simulations using experimental data. It is shown that EKF, UKF and EnKF are capable to provide accurate estimation results based on local point-wise temperature measurement. The estimation in addition captures the spatial-temporal evolution of moisture and maturity, which are relevant to evaluate the properties of the solidified product.

Future work will consider the validation of the property estimates using experimental data. Furthermore the extension to the full 3-dimensional case will be investigated towards the implementation of a closed-loop control concept for the imprinting of certain temperature profiles for curing and solidification.

## REFERENCES

- Benedix, O. (2011). *Adaptive numerical solution of state constrained optimal control problems*. Ph.D. thesis, Technische Universität München.
- Clauß, F., Ahrens, M.A., and Mark, P. (2022). Thermo-mechanical experiments on reinforced concrete beams: Assessing thermal, mechanical, and mixed impacts on fiber optic measurements. *Structural Concrete*, 23(6), 3521–3537.
- Evensen, G. (2003). The ensemble kalman filter: Theoretical formulation and practical implementation. *Ocean dynamics*, 53(4), 343–367.
- Fehling, E., Schmidt, M., Teichmann, T., Bunje, K., Bornemann, R., and Middendorf, B. (2005). *Schriftenreihe Baustoffe und Massivbau Structural Materials and Engineering Series Entwicklung, Dauerhaftigkeit und Berechnung Ultrahochfester Betone (UHPC)*. Technical report. URL <http://dnb.ddb.de>.
- Forman, P., Penkert, S., Kämper, C., Stallmann, T., Mark, P., and Schnell, J. (2020). A survey of solar concrete shell collectors for parabolic troughs. *Renewable and Sustainable Energy Reviews*, 134, 110–331.
- Fowkes, N., Mamboundou, H.M., Makinde, O., Ballim, Y., and Patini, A. (2004). Maturity effects in concrete dams. In D. Mason (ed.), *Proceedings of the Mathematics in Industry Study Group*, volume 1, 59–67.
- Gelb, A. et al. (1974). *Applied optimal estimation*. MIT press.
- Gillijns, S. et al. (2006). What is the ensemble Kalman filter and how well does it work? *Proceedings of the American Control Conference*, 2006, 4448–4453.
- Julier, S. and Uhlmann, J. (2004). Corrections to “unscented filtering and nonlinear estimation”. *Proceedings of the IEEE*, 92(12), 1958–1958.
- Löschmann, J. and Mark, P. (2022). Strengthening of beams or slabs using temperature induction. *Structural Concrete*, 23(5), 2770–2785.
- Myers, T. and Charpin, J. (2008). Modelling the temperature, maturity and moisture content in a drying concrete block. *Mathematics-in-Industry Case Studies*, 1.
- Olipitz, M. (2015). Paulifurt-bridge-design, planing and execution of a uhpc-shell-bridge. *Beton-und Stahlbetonbau*, 110(5), 365–373.
- Sagmeister, B. (2017). *Maschinenteile aus zementgebundenem Beton*. Beuth Verlag.
- Sanio, D., Alawieh, H., Bomholt, F., von Daake, H., Prenting, A., and Mark, P. (2021). Temporary post-anchoring of bar tendons by bond development of an anchoring system for transversely prestressed deck-slabs. *Beton-und Stahlbetonbau*, 116(10), 741–753.
- Schwarz, H.R. and Köckler, N. (2009). *Numerische Mathematik*. Springer-Verlag.
- Stindt, J., Forman, P., and Mark, P. (2021). Influence of rapid heat treatment on the shrinkage and strength of high-performance concrete. *Materials*, 14(15), 4102.
- Wan, E.A. and Van Der Merwe, R. (2000). The unscented Kalman filter for nonlinear estimation. In *IEEE 2000 Adaptive Systems for Signal Processing, Communications, and Control Symposium, AS-SPCC 2000*, 153–158.
- Welch, G. and Bishop, G. (2006). An Introduction to the Kalman Filter. *In Practice*, 7(1), 1–16.